

Critical Currents in Quasiperiodic Pinning Arrays: Chains and Penrose Lattices

Vyacheslav Misko^{1,2}, Sergey Savel'ev¹, and Franco Nori^{1,2}

¹ Frontier Research System, Institute of Physical and Chemical Research (RIKEN), Wako-shi, Saitama, 351-0198, Japan and
² MCTP, CSCS, Physics Department, University of Michigan, Ann Arbor, MI 48109-1040, USA

(Dated: June 22, 2018)

We study the critical depinning current J_c versus the applied magnetic flux Φ , for quasiperiodic (QP) chains and 2D arrays of pinning centers placed on the nodes of a five-fold Penrose lattice. In QP chains, the peaks in $J_c(\Phi)$ are determined by a sequence of harmonics of the long and short segments of the chain. The critical current $J_c(\Phi)$ has a remarkable self-similarity. In 2D QP pinning arrays, we predict analytically and numerically the main features of $J_c(\Phi)$, and demonstrate that the Penrose lattice of pinning sites provides an enormous enhancement of $J_c(\Phi)$, even compared to triangular and random pinning site arrays. This huge increase in $J_c(\Phi)$ could be useful for applications.

PACS numbers: 74.25.Qt

Recent progress in the fabrication of nanostructures has provided a wide variety of well-controlled vortex-confinement topologies, including different regular pinning arrays. A main fundamental question in this field was how to drastically increase vortex pinning, and thus the critical current J_c , using artificially-produced periodic Arrays of Pinning Sites (APS) [1, 2, 3, 4, 5]. The increase and, more generally, control of the critical current J_c in superconductors by its patterning (perforation) can be of practical importance for applications in micro-electronic devices.

A peak in the critical current $J_c(\Phi)$, for a given value of the magnetic flux per unit cell, say Φ_1 , can be engineered using a superconducting sample with a periodic APS with a matching field $H_1 = \Phi_1/A$ (where A is the area of the pinning cell), corresponding to one trapped vortex per pinning site. However, this peak in $J_c(\Phi)$, while useful to obtain, *decreases very quickly* for fluxes away from Φ_1 . Thus, the desired peak in $J_c(\Phi)$ is *too narrow* and not very robust against changes in Φ . It would be greatly desirable to have samples with APS with *many* periods (ideally infinite). This multiple-period APS sample would provide either very many peaks or an extremely broad peak in $J_c(\Phi)$, as opposed to just one (narrow) main peak (and its harmonics). We achieve this goal [a very broad $J_c(\Phi)$] here by studying samples with many built-in periods.

Here, we study vortex pinning by quasiperiodic (QP) chains and by 2D APS located on the nodes of QP lattices (e.g., a five-fold Penrose lattice) [6]. We show that the use of the 2D QP (Penrose) lattice of pinning sites results in a remarkable *enhancement* of $J_c(\Phi)$, as compared to other APS, including triangular and random APS. In contrast to superconducting networks, for which *only* the areas of the network plaquettes play a role [7], for vortex pinning by QP pinning arrays, the specific geometry of the elements which form the QP lattice *and* their arrangement (and not just the areas) are important, making the problem far more complicated.

Simulation.— We model a three-dimensional (3D)

slab, infinitely long in the z -direction, by a 2D (in the xy -plane) simulation cell with periodic boundary conditions. We perform simulated annealing simulations by numerically integrating the overdamped equations of motion (see, e.g., Ref. [8, 9]): $\eta \mathbf{v}_i = \mathbf{f}_i = \mathbf{f}_i^{vv} + \mathbf{f}_i^{vp} + \mathbf{f}_i^T + \mathbf{f}_i^d$. Here \mathbf{f}_i is the total force per unit length acting on vortex i , \mathbf{f}_i^{vv} and \mathbf{f}_i^{vp} are the forces due to vortex-vortex and vortex-pin interactions, respectively, \mathbf{f}_i^T is the thermal stochastic force, and \mathbf{f}_i^d is the driving force; η is the viscosity, which is set to unity. The force due to the vortex-vortex interaction is $\mathbf{f}_i^{vv} = \sum_j^{N_v} f_0 K_1(|\mathbf{r}_i - \mathbf{r}_j|/\lambda) \hat{\mathbf{r}}_{ij}$, where N_v is the number of vortices, K_1 is a modified Bessel function, λ is the penetration depth, $\hat{\mathbf{r}}_{ij} = (\mathbf{r}_i - \mathbf{r}_j)/|\mathbf{r}_i - \mathbf{r}_j|$, and $f_0 = \Phi_0^2/8\pi^2\lambda^3$. Here $\Phi_0 = hc/2e$. The pinning force is $\mathbf{f}_i^{vp} = \sum_k^{N_p} f_p \cdot (|\mathbf{r}_i - \mathbf{r}_k^{(p)}|/r_p) \Theta\left[\left(r_p - |\mathbf{r}_i - \mathbf{r}_k^{(p)}|\right)/\lambda\right] \hat{\mathbf{r}}_{ik}^{(p)}$, where N_p is the number of pinning sites, f_p (expressed in f_0) is the maximum pinning force of each short-range parabolic potential well located at $\mathbf{r}_k^{(p)}$, r_p is the range of the pinning potential, Θ is the Heaviside step function, and $\hat{\mathbf{r}}_{ik}^{(p)} = (\mathbf{r}_i - \mathbf{r}_k^{(p)})/|\mathbf{r}_i - \mathbf{r}_k^{(p)}|$. All the lengths (fields) are expressed in units of λ (Φ_0/λ^2). The ground state of a system of moving vortices is obtained by simulating the field-cooled experiments (e.g., [10]). For deep short-range (δ -like) potential wells, the energy required to depin vortices is proportional to the number of pinned vortices, $N_v^{(p)}$. Therefore, in this approximation, we can define the critical current as follows: $j_c(\Phi) = j_0 N_v^{(p)}(\Phi)/N_v(\Phi)$, where j_0 is a constant, and study the dimensionless value $J_c = j_c/j_0$. We use narrow potential wells as pinning sites, with $r_p = 0.04\lambda$ to 0.1λ . We have also performed dynamical simulations of J_c using a threshold criterion, i.e., J_c is obtained as the minimum current $J \propto f_1^d$ which depins the vortices. The results obtained using these two criteria are essentially equal [11], and here we use the “static” criterion defined above.

1D quasicrystal.— A QP chain [6] can be constructed by iteratively applying the Fibonacci rule ($L \rightarrow$

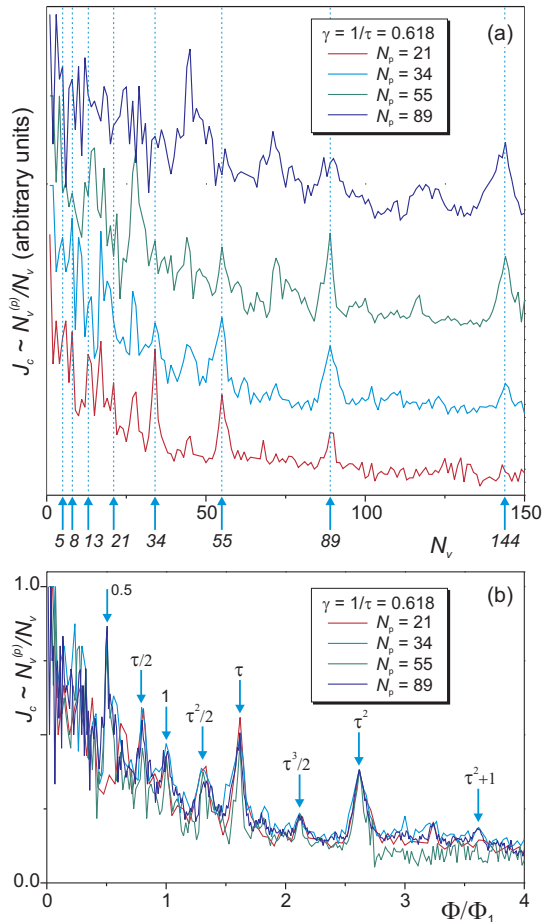


FIG. 1: (Color online) (a) The critical depinning current J_c , versus the number of vortices, $N_v \sim \Phi$, for 1D QP chains, $N_p = 21$ (red bottom line), $N_p = 34$ (second from the bottom blue line), $N_p = 55$ (green line), and $N_p = 89$ (dark blue top line), for $\gamma = a_S/a_L = 1/\tau$. Here we use: $f_p/f_0 = 1.0$ and $r_p = 0.1\lambda$. Independently of the length of the chain, the peaks include the sequence of successive Fibonacci numbers and their sub-harmonics. (b) The function $J_c(\Phi/\Phi_1)$ for the same 1D chains (using same colors). The curves for different chains display the same set of peaks, namely, at $\Phi/\Phi_1 = 1$ (first matching field) and $\Phi/\Phi_1 = 0.5$, as well as at the golden-mean-related values: $\Phi/\Phi_1 = \tau, \tau/2, (\tau + 1)/2 = \tau^2/2, (\tau^2 + \tau)/2 = \tau^3/2, \tau^2 = \tau + 1, \tau^2 + 1$. This behavior demonstrates the self-similarity of $J_c(\Phi)$.

$LS, S \rightarrow L$), which generates an infinite sequence of two line segments, long L and short S . For an infinite QP sequence [6], the ratio of the numbers of long to short segments is the golden mean $\tau = (1 + \sqrt{5})/2$. Let, e.g., $a_S = 1$ and $a_L = \tau$, where a_S and a_L are the lengths of the short and long segments, respectively. Then the position of the n th point where a new segment, either L or S , begins is determined by: $x_n = n + [n/\tau]/\tau$, where $[x]$ denotes the integer part of x . To study the critical depinning current J_c in QP pinning chains, we place pinning sites to the points where the L or S elements of the QP sequence link to each other.

The results of calculating $J_c(N_v)$ for chains of different

length and the same $\gamma = 1/\tau$ are shown in Fig. 1a. The plot clearly shows that, for sufficiently long chains, the positions of the main peaks in J_c , to a significant extent, do not depend on the length of the chain. The peaks form a Fibonacci sequence: $N_v = 13, 21, 34, 55, 89, 144$, and other “harmonics”: $N_v \cong 17, 27.5 (= 55/2), 44.5 (= 89/2)$, etc. Of course, longer chains allow to better reveal peaks for larger Fibonacci numbers. In Fig. 1b, the same curves are rescaled, normalized by the numbers of pins in each chain. The rescaled J_c curves reproduce each other and have many pronounced peaks for golden-mean-related values of Φ/Φ_1 (Φ_1 is the flux corresponding to the first matching field, H_1 , when $N_v = N_p$), as shown in Fig. 1b. Therefore, the same peaks of $J_c(\Phi)$, for different chains, are revealed before and after rescaling because of the self-similarity of $J_c(\Phi)$. The self-similarity of $J_c(\Phi)$ has also been studied in reciprocal k -space and will be presented elsewhere [11].

Penrose lattice.— Consider now a 2D QP APS, namely, an APS located at the nodes of a five-fold Penrose lattice. This lattice is a 2D QP structure, or quasicrystal, also referred to as Penrose tiling [6]. These structures possess a perfect local rotational (five- or ten-fold) symmetry, but do not have translational long-range order. The unusual self-similar diffraction pattern of a Penrose lattice exhibits a dense set of “Bragg” peaks because the lattice contains an infinite number of periods in it [6]. It is precisely this unusual property that is responsible for the striking $J_c(\Phi)$ ’s obtained here.

The structure of a five-fold Penrose lattice is presented in Fig. 2a. As an illustration only, a small five-fold symmetric fragment with 46 points is shown. According to specific rules, the points are connected by lines in order to display the structure of the Penrose lattice. The elemental building blocks are rhombuses with equal sides a and angles which are multiples of $\theta = 36^\circ$. There are two kinds of rhombuses: (i) those having angles 2θ and 3θ (so-called “thick”; shown empty in Fig. 2a), and (ii) rhombuses with angles θ and 4θ (so-called “thin”; filled in orange in Fig. 2a).

Let us analyze whether any specific matching effects can exist between the Penrose pinning lattice and the interacting vortices, which affect the magnetic-field dependence of the critical depinning current $J_c(\Phi)$ (Fig. 2). Quasicrystalline patterns are intrinsically *incommensurate* with the flux lattice for *any* value of the magnetic field [7], therefore, in contrast to periodic (e.g., triangular or square) pinning arrays, one might *a priori* assume a *lack* of sharp peaks in $J_c(\Phi)$ for QP APS. However, the existence of many periods in the Penrose lattice can lead to a hierarchy of matching effects for certain values of the applied magnetic field, resulting in strikingly-broad shapes for $J_c(\Phi)$. These could be valuable for applications demanding unusually broad $J_c(\Phi)$ ’s.

To match the vortex lattice on an entire QP APS, the specific geometry of the elements which form the QP lattice is important, as well as their arrangement. While the sides, a , of the rhombuses are equal, the distances

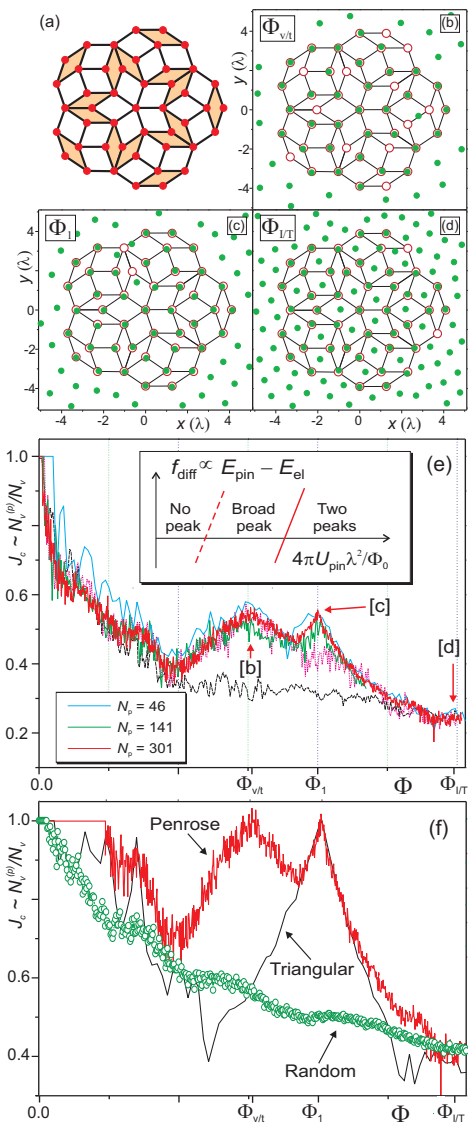


FIG. 2: (Color online) (a) An example of a five-fold Penrose lattice, consisting of “thick” and “thin” rhombuses. (b to d) The location of vortices (green dots) and the Penrose-lattice APS (red open circles connected by black lines) for: (b) $\Phi = \Phi_{\text{vacancy/thin}} \equiv \Phi_{v/t} = 0.757 \Phi_1$, vortices occupy all the pinning sites except those in one of the two vertices of each “thin” rhombus; (c) $\Phi = \Phi_1$, N_v coincides with N_p ; (d) $\Phi = \Phi_{\text{interstitial/thick}} \equiv \Phi_{i/T} = 1.482 \Phi_1$, vortices occupy both the pinning sites and the interstitial positions inside each “thick” rhombus. Here $f_p/f_0 = 2.0$, $r_p = 0.1\lambda$. (e) The $J_c(\Phi \sim N_v)$ for Penrose-lattice arrays with $N_p = 46, 141, 301$. The data points [b], [c], [d] refer to snapshots in 2b, 2c, 2d, respectively. The peak [c] at Φ_1 is suppressed for weaker pinning (magenta dotted J_c curve). Eventually, all the main peaks disappear for sufficiently weak pins (black dashed curve). The inset shows the dimensionless difference, f_{diff} , of the pinning and the elastic energies versus the pinning-to-interaction energy ratio, for the broad J_c peak at $\Phi_{v/t}$ (red dashed line) and for Φ_1 (red solid line). Only $f_{\text{diff}} > 0$ gives stable peaks in J_c . (f) The $J_c(\Phi)$ for a 301-sites Penrose-lattice (red solid line), (recalculated for flux only on the Penrose area, A_P), triangular (black solid line) and random (green open circles and solid line) pinning arrays.

between the nodes are *not* equal. The lengths of the diagonals of the rhombuses (Fig. 2a) are: $1.176a$, $\tau a \approx 1.618a$ (for the thick rhombus), $(\tau - 1)a = a/\tau \approx 0.618a$, and $1.902a$ (for the thin rhombus). Based on these distances, we can predict matching effects (and corresponding features of the function $J_c(\Phi)$) for the Penrose-lattice APS.

First, there is a “first matching field” (we denote the corresponding flux as Φ_1) when each pinning site is occupied by a vortex (Fig. 2c). Although the sides of all the rhombuses are equal to each other, nevertheless this matching effect is not expected to be accompanied by a sharp peak. Instead, it is a broad maximum (peak [c] in Fig. 2e) involving three kinds of local “commensurability” effects of the flux lattice: with the rhombus side a ; with the short diagonal of a thick rhombus, $1.176a$, which is close to a ; and with the short diagonal of a thin rhombus, which is $a/\tau \approx 0.618a$. For the overall square cell used, some of the vortices are outside the Penrose sample; these mimic the applied magnetic field and determine the average vortex density in the entire cell. Because of the additional vortices outside the Penrose APS, our computed $J_c(\Phi)$ is reduced by a factor $\eta = A_P/A \approx 0.575$ (see Fig. 2e), where A_P and A are the areas of the Penrose lattice and of the cell.

Another matching (Fig. 2b) is related with the filling of all the pinning sites on the vertices of the thick rhombuses and only *three out of four* of the pinning sites on the vertices of thin rhombuses, i.e., one of the pinning sites on the vertices of the thin rhombuses is empty. For this value of the flux, matching conditions are fulfilled for *two* close distances, a (the side of a rhombus) and $1.176a$ (the short diagonal of a thick rhombus), but are not fulfilled for the short diagonal, a/τ , of the thin rhombus. Therefore, this 2D QP feature is related to τ , although not in such a direct way as in the case of a 1D QP pinning array. This 2D QP matching results in a very wide maximum (arrow [b] in Fig. 2e) of the function $J_c(\Phi)$. The position of this broad maximum (denoted here by $\Phi_{\text{vacancy/thin}} \equiv \Phi_{v/t} = 0.757 \Phi_1$) could be found as follows. The ratio of the numbers of thick and thin rhombuses is determined by the Fibonacci numbers and in the limit of large pinning arrays, $N_p \rightarrow \infty$, this ratio tends to τ . The number of unoccupied pinning sites is governed by the number of thin rhombuses. However, some of the thin rhombuses are separated from other thin rhombuses by a single thick one (*single* thin rhombuses; see Fig. 2a), while some of thin rhombuses have common sides with each other (orange arrow-shaped *double* thin rhombuses in Fig. 2a). Therefore, the number of vacancies (i.e., unoccupied pins) is then the number of single thin rhombuses N_{rh}^s plus one half of the number N_{rh}^d of “double” thin rhombuses, $N_p^{\text{un}}(\Phi_{v/t}) = N_{\text{rh}}^s + N_{\text{rh}}^d/2$, where N_p^{un} is the number of unoccupied pinning sites at $\Phi = \Phi_{v/t}$.

For higher vortex densities ($\Phi = \Phi_{\text{interstitial/thick}} \equiv \Phi_{i/T} = 1.482 \Phi_1$) a single interstitial vortex is inside each thick rhombus (see Fig. 2d). These interstitial vortices can easily move; thus J_c has no peak at $\Phi_{i/T}$. The position of this feature is determined by the number of vor-

tices at $\Phi = \Phi_1$, which is $N_v(\Phi) = N_p$, plus the number of thick rhombuses, $N_{\text{rh}}^{\text{thick}} = N_{\text{rh}}/\tau$.

In order to better understand the structure of $J_c(\Phi)$ for the Penrose pinning lattice, we compare the elastic E_{el} and pinning E_{pin} energies of the vortex lattice at H_1 and at (the lower field) $H_{v/t}$, corresponding to the two maxima of J_c (Figs. 2e,f). Vortices can be pinned if the gain $E_{\text{pin}} = U_{\text{pin}} \beta n_{\text{pin}}$ of the pinning energy is larger than the increase of the elastic energy [12] related to local compressions: $E_{\text{el}} = C_{11}[(a_{\text{eq}} - b)/a_{\text{eq}}]^2$. The shear elastic energy ($\propto C_{66}$) provides the same qualitative result [11]. Here, $U_{\text{pin}} \sim f_p r_p$, n_{pin} is the density of pinning centers, $\beta(H \leq H_1) = H/H_1 = B/(\Phi_0 n_{\text{pin}})$, and $\beta(H > H_1) = 1$ is the fraction of occupied pinning sites ($\beta = 1$ for $H = H_1$, and $\beta = 0.757$ for $H = H_{v/t}$), $a_{\text{eq}} = (2/\sqrt{3}\beta n_{\text{pin}})^{1/2}$ is the equilibrium distance between vortices in the triangular lattice, b is the minimum distance between vortices in the distorted pinned vortex lattice ($b = a/\tau$ for $H = H_1$ and $b = a$ for $H = H_{v/t}$), and $C_{11} = B^2/[4\pi(1 + \lambda^2 k^2)]$ is the compressibility modulus for short-range deformations [12] with characteristic spatial scale $k \approx (n_{\text{pin}})^{1/2}$. The dimensionless difference of the pinning and elastic energies is $E_{\text{pin}} - E_{\text{el}} = \beta f_{\text{diff}} n_{\text{pin}} \Phi_0^2 / (4\pi \lambda^2)$, where $f_{\text{diff}} = 4\pi \lambda^2 U_{\text{pin}} / \Phi_0^2 - \beta \left[1 - b (\beta \sqrt{3} n_{\text{pin}} / 2)^{1/2} \right]^2$. Near matching fields, J_c has a peak when $f_{\text{diff}} > 0$ (and no peak when $f_{\text{diff}} < 0$). Since only two matching fields provide $f_{\text{diff}} > 0$, then our analysis explains the two-peak structure observed in J_c shown in Figs. 2e,f. For instance, for the main matching fields: $f_{\text{diff}}(\Phi_{v/t}) \approx 0.0056$, $f_{\text{diff}}(\Phi_1) \approx 0.0058$, and $f_{\text{diff}}(\Phi_{i/T}) \approx -0.09$. Note that for weaker pinning, the two-peak structure gradually turns into one very broad peak, and eventually zero peaks for weak enough pinning (see Fig. 2e). The J_c peaks corresponding to higher matching fields are strongly suppressed because of the fast increase ($\propto B^2$) of the compressibility modulus C_{11} and, thus, the elas-

tic energy with respect to the pinning energy; the latter cannot exceed the maximum value $U_{\text{pin}} n_{\text{pin}}$. The subharmonic peaks of J_c , which could occur for lower fields $H < H_{v/t}$, are also suppressed due to the increase of C_{11} associated with the growing spatial scales $1/k$ of the deformations.

For comparison, we show the $J_c(\Phi)$ for the Penrose lattice (itself, i.e. calculated only for A_P), triangular and random pinning arrays (Fig. 2f). The latter is an average over five realizations of disorder. Notice that the QP lattice leads to a very broad and potentially useful *enhancement* of the critical current $J_c(\Phi)$, even compared to the triangular or random APS. The remarkably broad maximum in $J_c(\Phi)$ is due to the fact that the Penrose lattice has *many* (infinite, in the thermodynamic limit) periodicities built in it [6]. In principle, each one of these periods provides a peak in $J_c(\Phi)$. In practice, like in quasicrystalline diffraction patterns, only few peaks are strong. This is also consistent with our study. Furthermore, the pinning parameters can be adjusted by using as pinning centers either antidots “drilled” in the film [1, 3], or blind antidots [4] of different depths and radii. Thus, our results could be observed experimentally.

Conclusions.— The critical depinning current $J_c(\Phi)$ was studied in 1D QP chains and in 2D QP arrays (the five-fold Penrose lattice) of pinning sites. A hierarchical and self-similar $J_c(\Phi)$ was obtained. We physically analyzed all the main features of $J_c(\Phi)$. Our analysis shows that the QP lattice provides an unusually broad critical current $J_c(\Phi)$, that could be useful for practical applications demanding high J_c 's over a wide range of fields. Our proposal can be easily extended, *mutatis mutandi*, to other related systems, including colloidal suspensions interacting with pinning traps provided by arrays of optical tweezers [13].

This work was supported in part by ARDA and NSA under AFOSR contract F49620-02-1-0334; and by the US NSF grant No. EIA-0130383.

-
- [1] M. Baert *et al.*, Phys. Rev. Lett. **74**, 3269 (1995); V.V. Moshchalkov *et al.*, Phys. Rev. B **54**, 7385 (1996).
[2] J.E. Villegas *et al.*, Science **302**, 1188 (2003); Phys. Rev. B **68**, 224504 (2003); M.I. Montero *et al.*, Europhys. Lett. **63**, 118 (2003).
[3] A.M. Castellanos *et al.*, Appl. Phys. Lett. **71**, 962 (1997); R. Wördenweber *et al.*, Phys. Rev. B **69**, 184504 (2004).
[4] L. Van Look *et al.*, Phys. Rev. B **66**, 214511 (2002).
[5] A.V. Silhanek *et al.*, Phys. Rev. B **67**, 064502 (2003).
[6] *Quasicrystals*, Ed. J.-B. Suck, M. Schreiber, P. Häussler (Springer, Berlin, 2002).
[7] A. Behrooz *et al.*, Phys. Rev. B **35**, 8396 (1987); F. Nori *et al.*, *ibid.* **36**, 8338 (1987); **37**, R2364 (1988); **39**, 2134 (1989).
[8] C. Reichhardt *et al.*, Phys. Rev. B **57**, 7937 (1998).
[9] B.Y. Zhu *et al.*, Phys. Rev. Lett. **92**, 180602 (2004); Physica E **18**, 318, 322 (2003); Phys. Rev. B **68**, 014514 (2003); Physica C **388-389**, 665 (2003); **404**, 260 (2004).
[10] K. Harada *et al.*, Science **274**, 1167 (1996).
[11] V.R. Misko, S. Savel'ev, and F. Nori, unpublished.
[12] E.H. Brandt, Rep. Prog. Phys. **58**, 1465 (1995).
[13] J.C. Crocker and D.G. Grier, J. Colloid Interface Sci. **179**, 298 (1996).